Analytica Chimica Acta 1384 (2026) 344982

Contents lists available at ScienceDirect

Analytica Chimica Acta

journal homepage: www.elsevier.com/locate/aca

Towards fiber optic chemical sensors for 1,3-butadiene detection in Titan's hydrocarbon lakes

Diogo Gonçalves [a,b], Cláudia Ribeiro [a], João P.C. Tomé [a], Bruno Pedras [b,1], Zita Martins [a,*,1]

[a] Centro de Química Estrutural, Institute of Molecular Sciences, And Department of Chemical Engineering, Instituto Superior Técnico, Universidade de Lisboa, Av. Rovisco Pais 1, 1049-001, Lisbon, Portugal

[b] Institute for Bioengineering and Biosciences, Associate Laboratory i4HB-Institute for Health and Bioeconomy, and Department of Chemical Engineering, Instituto Superior Técnico, Universidade de Lisboa, Av. Rovisco Pais 1, 1049-001, Lisbon, Portugal

HIGHLIGHTS

- Tetrazine fluorescent indicator for 1,3-butadiene on Titan's surface.
- Sensing strategy based on an inverse electron-demand Diels-Alder click reaction.
- The sensor operates when immobilized in polystyrene, apt for apolar environments.
- Fluorescence-based fiber optic sensors can contribute to space exploration.
- Fiber optic chemical sensing is space-ready and of swift and cheap development.

GRAPHICAL ABSTRACT

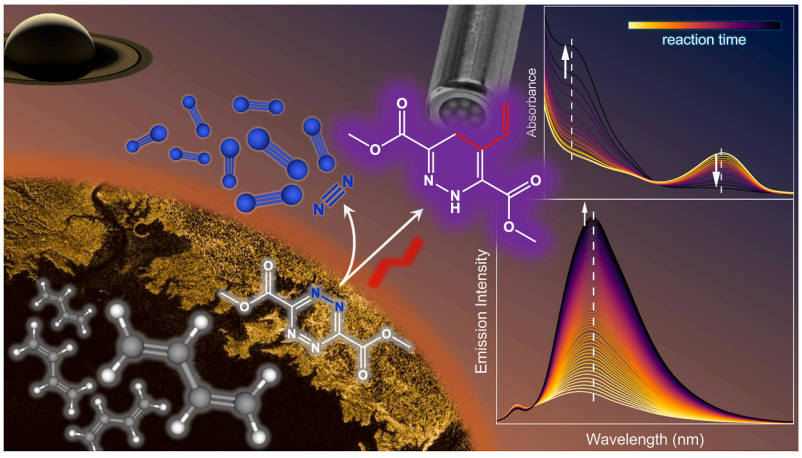

ARTICLE INFO

Handling Editor: Prof Rebecca Lai

Keywords:
1,3-Butadiene
Fiber optic chemical sensors
Fluorescence sensing
Space instrumentation
iEDDA
Titan

ABSTRACT

Background: Fiber optic chemical sensors (FOCS) can be rapidly integrated in future instrument suites for *in-situ* extraterrestrial chemical characterizations. At low development and deployment costs, they can complement the analysis of more capable instruments. The contribution of FOCS can best be exemplified by the detection of 1,3-butadiene in Titan. This analyte is an unsaturated hydrocarbon of relevance for Titan's atmospheric chemistry and geology, but its detection poses challenges for current spectroscopy and mass spectrometry space instruments. Here, we report the design of the sensing core of a future space-mission-ready FOCS tailored to detect 1,3-butadiene in Titan's hydrocarbon environments.

Results: We report the discovery and characterization of the first fluorescent indicator for 1,3-butadiene. The off-on detection strategy is based on an inverse electron demand Diels-Alder click-reaction between the analyte and

* Corresponding author.
E-mail address: zita.martins@tecnico.ulisboa.pt (Z. Martins).
[1] These authors share senior authorship.

https://doi.org/10.1016/j.aca.2025.344982
Received 14 October 2025; Received in revised form 19 November 2025; Accepted 1 December 2025
Available online 4 December 2025

a tetrazine indicator, yielding emissive 1,4-dihydropyridazine derivatives, as confirmed by NMR. Excitation above 415 nm enables the selective detection of 1,3-butadiene against competing unsaturated hydrocarbons present in Titan. The sensor exhibited a limit of detection of 1.1 ppm (mol mol^{-1}) and a linear response up to the expected saturation concentration in Titan's lakes. Furthermore, the fast and irreversible reaction between the tetrazine indicator and 1,3-butadiene provides rapid sensor responses that increase with temperature. Operating the sensor at high temperatures also mitigates competing photobleaching reactions. The immobilization of the indicator in polystyrene membranes maintained its detection capability for 1,3-butadiene dissolved in hexane, an apolar solvent analogous to Titan's hydrocarbon lakes.

Significance: The demonstration of the solid-state functionality of the indicator marks the last step towards its integration with space-qualified instrumentation. This proof-of-principle detection of 1,3-butadiene highlights the potential of fluorescence sensing for probing exotic planetary environments. Fiber optic architectures are ideal platforms for adapting fluorescence-based chemical sensing strategies to the *in-situ* characterization of extraterrestrial sites.

1. Introduction

Spaceflight exerts strong aggressions on payload suites: mechanical stress during launch, energetic irradiation whilst in space, extreme pressure and temperature ranges when landed in extraterrestrial worlds, while adhering to stringent mass, volume, power and data rate limitations. To such challenging conditions, fiber optic sensors have proven to be suitable instruments. They are not only immune to electrical and magnetic interference but also easily miniaturized, highly robust, geometrically flexible, and energy efficient [1–4]. These and other advantages have led to a two-decade long history of development towards their integration in spacecrafts, whose historical perspective from the European Space Agency (ESA) was recently reviewed by McKenzie et al. [5]. Outstanding implementations of fiber optic sensing include the Basic Angle Measurement (BAM) sensor on ESA's GAIA mission [6] and the recent JUICE magnetometer (J-MAG) on ESA's JUICE mission [7].

Fiber optic sensors tuned to the detection of chemical substances – fiber optic chemical sensors (FOCS) – have been adopted for monitoring environmental quality in several working environments [4,8,9]. Still, such FOCS [8,10–12] are yet to be deployed in space missions or considered for those of the future [13–15]. In a FOCS, an optical fiber guides light whose properties are altered by chemical interactions. Albeit outstanding work has been reported on intrinsic FOCS, where the optical fiber itself senses the analyte – by replacing or coating the fiber cladding with a chemically selective material [16–18] –, in our laboratory we have focused on extrinsic FOCS architectures. In these, the optical fiber solely transports light to and from a responsive material placed at its tip. The external material, commonly a plasticized polymeric membrane or a sol-gel glass [19], reacts specifically to the analyte, signaling its presence by spectroscopic variations. The extrinsic architecture ultimately grants higher tunability to maximize the sensor specificity. Our team also focused on fluorescence sensing strategies to maximize the sensor sensitivity; in these, the responsive material has its emission profile, wavelength, lifetime or intensity changed in the presence of the analyte [9,20–22].

The simplicity of FOCS makes them cheap to assemble. Also, their assemblage from components with over two decades of spacecraft-tailored development [5] may fast-track them through spaceflight qualification. Further easing their implementation, FOCS can be readily incorporated in extant fluorescence spectroscopy instruments, helping to extend the capabilities of the latter. Fluorescence and Raman sensing have recently, and for the first time, been included in *in-situ* scientific payloads, through the SHERLOC instrument currently onboard the Mars 2020 rover [23–25]. Its instrumentation has since been adapted to the search for biosignatures in extraterrestrial icy environments [26], and, thanks to its ease of miniaturization, fluorescence and Raman spectroscopies shall become prevalent in future scientific instrument suites [15]. FOCS may be integrated into such instruments as semiquantitative complementary detectors of analytes of high scientific interest – tailored to address minimal scientific requirements. They can also assist with the calibration of the same instruments and do so at low costs of development and deployment. Not only they could assist fluorescence and Raman instruments in gathering sufficient chemical information to identify chemical species [15] but also – although still integrated into fluorescence instrumentation – validate key results and address limitations of more capable techniques. In one envisioned application, FOCS could address the difficulty of gas chromatography-mass spectrometry (GC-MS) in distinguishing hydrocarbons of interest from their isomers on a complex hydrocarbon matrix as Titan's methane/ethane lakes are expected to be [27–30]. Such hydrocarbon selectivity is a challenge for both spectroscopy and mass spectrometry instruments, a challenge which FOCS can promptly address. To demonstrate it, in this manuscript we propose to develop a FOCS dedicated to the detection of 1,3-butadiene (a C_4H_6 isomer) in the hydrocarbon lakes of Titan.

1,3-Butadiene is modeled to be one of the hydrocarbon products of Titan's atmospheric photochemistry [31,32]. Upon deposition on the Saturnian moon's surface, and after precipitation from the surface hydrocarbon lakes, it may partake in non-covalent interactions sufficiently strong to constitute cryogenic organic "rocks" [33]. Also, being a conjugated hydrocarbon molecule – the smallest and likely the most common on Titan [32,34] –, 1,3-butadiene can absorb down to UVC photons [35,36] to produce ethylene (C_2H_4) or propyne (C_3H_4) from its photolysis [32], and thus contribute to Titan's complex atmospheric photochemistry. The high reactivity of 1,3-butadiene may also enable it to undergo gas-phase thermal reactions on Titan's stratosphere, where temperatures may reach up to about 180 K [37]. Understanding the distribution of 1,3-butadiene on Titan's surface would inform Titan's organic geology and photochemical models. Still, to the extent of our knowledge, 1,3-butadiene was not yet detected on this moon [38].

As far as we are aware, no fluorescence-based sensors for 1,3-butadiene were yet reported or commercialized. From extant sensors, none operates in solution. In this work, we sought a molecular indicator for 1,3-butadiene which could be immobilized in a responsive membrane and so constitute the sensing core of a future 1,3-butadiene fluorescence FOCS in hydrocarbon solutions. A preliminary screening of the Diels-Alder reaction of 1,3-butadiene – acting as dienophile – with 27 dienes revealed that 1,2,4,5-tetrazine derivatives were promising indicators (Table S1). We expect these to react through the Carboni-Lindsey mechanism [39], an inverse electron demand Diels–Alder (iEDDA) click-reaction [40,41], explored at length for its mild-conditions, catalyst-free and biorthogonal labelling capabilities [42–46]. For our purposes, this mechanism offers selectivity, speed, and irreversibility [47], thus constituting an ideal chemodosimeter sensing strategy [48–51]. Specifically, the defining irreversibility of chemodosimeters makes the sensor response cumulate over exposure time, enabling the detection of very low analyte concentrations [52], key for our envisioned application given the unknown – but expectedly low – concentrations of 1,3-butadiene in Titan's lakes. Also, the only by-product of this click-reaction is N_2, 95 % of Titan's atmosphere, ensuring an innocuous chemical detection on this moon. In summary, we have explored 1,2,4,5-tetrazines as putative fluorescence indicators for 1,3-butadiene, as reported below. This way, we describe the

preliminary laboratory work towards the first space-mission-dedicated FOCS, intended to demonstrate that this sensing technology can complement future instrument suites for *in-situ* chemical characterizations in extraterrestrial environments.

2. Methods and materials

2.1. Chemicals and reagents

The tested indicators 3,6-bis(methoxycarbonyl)-1,2,4,5-tetrazine, 3,6-di-2-pyridyl-1,2,4,5-tetrazine (96.0 %), methyltetrazine-NHS ester (2,5-dioxo-1-pyrrolidinyl 4-(6-methyl-1,2,4,5-tetrazin-3-yl)benzeneacetate) (95.0 %), (4-(1,2,4,5-tetrazin-3-yl)phenyl)methanamine hydrochloride (95.0 %), (4-(6-methyl-1,2,4,5-tetrazin-3-yl)phenyl) methanamine hydrochloride (97.0 %), 3,6-bis(methylthio)-1,2,4,5-tetrazine (95.0 %), 3,6-diphenyl-1,2,4,5-tetrazine, and 3,6-bis(2-chlorophenyl)-1,2,4,5-tetrazine (98.0 %) were obtained from Sigma-Aldrich; 3,6-dichloro-1,2,4,5-tetrazine (97.0 %), 3,6-dimethyl-1,2,4,5-tetrazine (98.0 %), and 3,6-di(4-pyridyl)-1,2,4,5-tetrazine (98.0 %) were obtained from TCI. 1,3-Butadiene (ca. 15 % in hexane) and 1-pentyne (98.0 %) were obtained from TCI. Cyclopentene (97 %), *cis*-2-hexene (96 %), and 1-hexene (99 %) were obtained from Thermo Scientific Chemicals. The following solvents were used without further purification: acetonitrile (Sigma-Aldrich, 99.9 %), water (Sigma-Aldrich, HPLC grade), and tetrahydrofuran (Acros Organics, 99.5 %). Column chromatography was performed using Al_2O_3 (63–200 μm, Merck).

2.2. Indicator screening and general considerations for **tz-1** experiments

The reactivity of 1,3-butadiene with the putative tetrazine indicators was evaluated as follows. Each tetrazine was dissolved in a glass vial in 2 ml of acetonitrile to give a 10 mM solution. Water was added dropwise (≤10 drops) to ensure the dissolution of tetrazines 3,6-di(4-pyridyl)-1,2,4,5-tetrazine, 3,6-di(2-pyridyl)-1,2,4,5-tetrazine, (4-(1,2,4,5-tetrazin-3-yl)phenyl)methanamine, and (4-(6-methyl-1,2,4,5-tetrazin-3-yl) phenyl)methanamine. 50 μl of 1,3-butadiene (ca. 15 % w w^{-1} in hexane) was then added to the dissolved tetrazines, amounting to 4.5 equivalents relative to the latter. The vial was sealed and magnetically stirred at room temperature for 2 h. After this period, a 30 μl aliquot was diluted 100-fold with acetonitrile (final volume 3 ml), and its UV–Vis absorption and fluorescence emission spectra were recorded. The spectra were compared to those of an aliquot taken prior to the addition of 1,3-butadiene. The reactivity of 1,3-butadiene with tetrazines **tz-1–3** was confirmed at least three times and compared against appropriate controls (in the absence of 1,3-butadiene). All further experiments with **tz-1** (3,6-bis(methoxycarbonyl)-1,2,4,5-tetrazine) were performed in acetonitrile to ensure its dissolution. Details on concentration, reaction times and other sensing procedures are described throughout the results section.

Steady-state excitation and emission spectra were recorded with a modular spectrofluorometer (HORIBA Scientific) equipped with a 450-W xenon arc lamp and a R928 photomultiplier (PMT) detector (Hamamatsu). Our sample holder was mounted onto a thermoelectric module, driven by an LFI-3751 temperature controller (Wavelength Electronics), providing direct thermal regulation during the temperature sensitivity experiments (section 3.5). Settings configuration and data collection were performed using the FluorEssence software. The fluorescence of polymeric membranes was measured in front-face geometry. UV–Vis absorption measurements were performed using a Shimadzu UV-2600i UV–Vis spectrophotometer (Shimadzu Corporation). Acetonitrile was used as a blank reference in all solution samples. An empty Mylar® sheet was used as reference when measuring the absorption spectra of polymeric membranes, which were always placed perpendicular to the beam path. All absorption spectra were collected using the LabSolutions UV–Vis software.

2.3. Nuclear magnetic resonance (NMR)

^1H and ^{13}C NMR spectra were recorded on a Bruker 400 MHz Avance III NMR spectrometer at 400.13 and 100.58 MHz, respectively. Samples were dissolved in deuterated chloroform ($CDCl_3$, 99.8 %, TCI). Chemical shifts were referenced to the residual solvent signals and reported as δ-values in ppm. The *J* coupling constants are reported in Hz. Data were collected using the TopSpin (Bruker) software.

2.4. Fluorescence lifetime measurement

Fluorescence lifetimes were measured through Time-Correlated Single Photon Counting (TCSPC), carried out on a HORIBA DeltaFlex™ TCSPC system (HORIBA Scientific) using as excitation source a DeltaDiode-360 pulsed laser (HORIBA Scientific), at a 25-MHz repetition rate. Emission was detected with a PPD-900 detector (HORIBA Scientific), 20 ps response time, at the emission maximum of each reaction product. The instrument response was measured by the scattering from a dilute colloidal silica suspension (LUDOX®) in a quartz cuvette at the excitation wavelength. Data were collected with the EzTime software, and all decays were fitted by iterative reconvolution with the IRF, given the short lifetime of our excited state products. The fluorescence lifetimes were calculated after modelling the intensity decay response (I) through the sum of up to two exponential decays, each convoluted with the instrument response function modeled with a gaussian function (IRF) (Equation (1)):

$$I(t) = y_0 + IRF(t) * \sum_{i}^{n=2} A_i e^{\frac{t-t_0}{\tau_i}} \quad (1)$$

where y_0 is the signal baseline, A_i the amplitude of the *i*-decay, τ_i the lifetime of the *i*-decay, and t_0 the time point at which all dynamics begin. The reported errors are the standard error from fitting the raw data to this model and were propagated to the calculation of the average lifetime. Both the intensity (τ_{int}) and amplitude (τ_{amp}) average lifetimes were calculated as follows (Equation (2)):

$$\tau_{int} = \frac{\sum_{i=1}^{n} \alpha_i \tau_i^2}{\sum_{i=1}^{n} \alpha_i \tau_i};\ \tau_{amp} = \sum_{i=1}^{n} \alpha_i \tau_i \quad (2)$$

with α_i the normalized amplitudes (Equation (3)):

$$\alpha_i = \frac{A_i}{A_1 + A_2} \quad (3)$$

2.5. Limit of detection determination

To determine the limit of detection (LOD) of 1,3-butadiene using the **tz-1** indicator, we tested their reaction at different 1,3-butadiene concentrations. A 1.83 mM 1,3-butadiene stock solution was prepared by diluting the commercial 1,3-butadiene solution 1000-fold with acetonitrile to a final volume of 10 ml. The stock solution was stored in a glass vial sealed with a screw cap fitted with a PTFE/silicone septum. A 14.38 mM **tz-1** working solution was also prepared by dissolving 17.1 mg of the compound in 6 ml of acetonitrile.

The sensing reactions were carried out in sealed glass vials, under stirring, for 24 h. The initial **tz-1** concentration was kept constant at 10.07 mM, while the 1,3-butadiene concentration was varied between 0, 50, 100, 200, and 500 μM. The reaction mixtures were prepared by combining 0.7 ml of the **tz-1** solution with 0, 27, 55, 109, or 273 μl of the 1,3-butadiene solution to achieve the 0, 50, 100, 200, and 500 μM concentrations, respectively. The total reaction volume was adjusted to 1 ml with pure acetonitrile. The 1,3-butadiene solution was added last to initiate the reaction timing. All 1,3-butadiene solutions were handled with glass syringes, rinsed and dried between uses.

After 24 h, a 100 μl aliquot of each reaction mixture was diluted 30-fold with acetonitrile (to a final volume of 3 ml) for spectroscopic analysis. UV–Vis absorption and fluorescence emission spectra were recorded for each sample. The dilution factor was selected to ensure that the absorbance at the excitation wavelength (333 nm) in the most concentrated reaction (500 μM) did not exceed A = 0.1, thereby minimizing inner filter effects from the reabsorption of emitted light ($\lambda_{em,max}$ = 449 nm) by the **tz-1** indicator ($\lambda_{abs,max}$ = 516 nm). The emission intensity at 449 nm was averaged over three measurements, each integrated over 1 s. The calibration curve was obtained by a linear regression analysis of the emission intensity versus analyte concentration. The LOD was calculated as three times the standard deviation of the emission intensity of three independent blank (0 μM) samples divided by the slope of the calibration curve.

2.6. Tz-1 immobilization in a polystyrene film

12.1 mg of **tz-1** (30.5 mM) and 152.5 mg of polystyrene pellets were dissolved in 2 ml and 1.5 ml of tetrahydrofuran (THF), respectively. Both solutions were close to saturation and only dissolved completely upon sonication. The solutions of **tz-1** and polystyrene were thoroughly mixed at a 3:1 ratio. Approximately 0.5 ml of this mixture were pipetted onto a 1 × 4 cm^2 Mylar® sheet. The solvent was then slowly evaporated in an oven at 40 °C until the film was completely set. During evaporation, the sheet was covered by an upside-down beaker, key to ensure a homogeneous distribution of the molecule in the polystyrene film, and of the latter in the Mylar® sheet. For reference and control purposes, an empty polystyrene film was prepared through the same protocol although the polystyrene solution was instead mixed with a pure THF solution, at the same (3:1) ratio.

3. Results and discussion

3.1. 1,2,4,5-Tetrazine screening and detection scheme

We evaluated whether 1,2,4,5-tetrazine derivatives could react with 1,3-butadiene fast enough and, in so doing, produce significant spectroscopic differences to act as indicators for the latter. We screened the reactivity of eleven tetrazine derivatives, eight of which symmetrically substituted (Scheme 1). Tetrazines **tz-1–3** reacted with 1,3-butadiene (Fig. 1), as repeatedly confirmed through changes in their absorption and emission spectra. From these, only 3,6-bis(methoxycarbonyl)-1,2,4,5-tetrazine (**tz-1**) reacted to completion in the allotted 2-h reaction time. Upon further testing we understood that the reaction with **tz-1** was complete in less than 10 min, at the conditions we performed the screening (section 2.2). Monitoring the reaction mixture absorption spectrum as the reaction progressed, we measured a decrease in the tetrazine absorption band at 516 nm and a pronounced increase at 333 nm, signaling the formation of a new compound (Fig. 2a). Consistent with it, the reaction mixture transformed from a tetrazine-characteristic red to a pale-yellow coloration. Crucially, the excitation at the new absorption band (with maximum at 333 nm) produced a new emission band with maximum at 449 nm (Fig. 2b). By measuring the excitation spectrum – collecting the emission at the new maximum (449 nm) – we could reconstruct the new absorption band (Fig. S1), suggesting that the emitting compound was the only absorbent reaction product. That observation is consistent with the quantitative (i.e., 100 %) yields reported for this reaction [47,53] and with our NMR analysis (section 3.2). The emitting reaction product demonstrated a fluorescence quantum yield of Φ = 0.013, as detailed in section S3, and an exceptionally high Stokes shift ($\lambda_{em,max} - \lambda_{abs,max}$) of 116 nm, a most desirable feature for a fluorescence sensing solution. Furthermore, the new emission band is more energetic than the **tz-1** $S_1 \leftarrow S_0$ absorption at 516 nm (Fig. 2), and

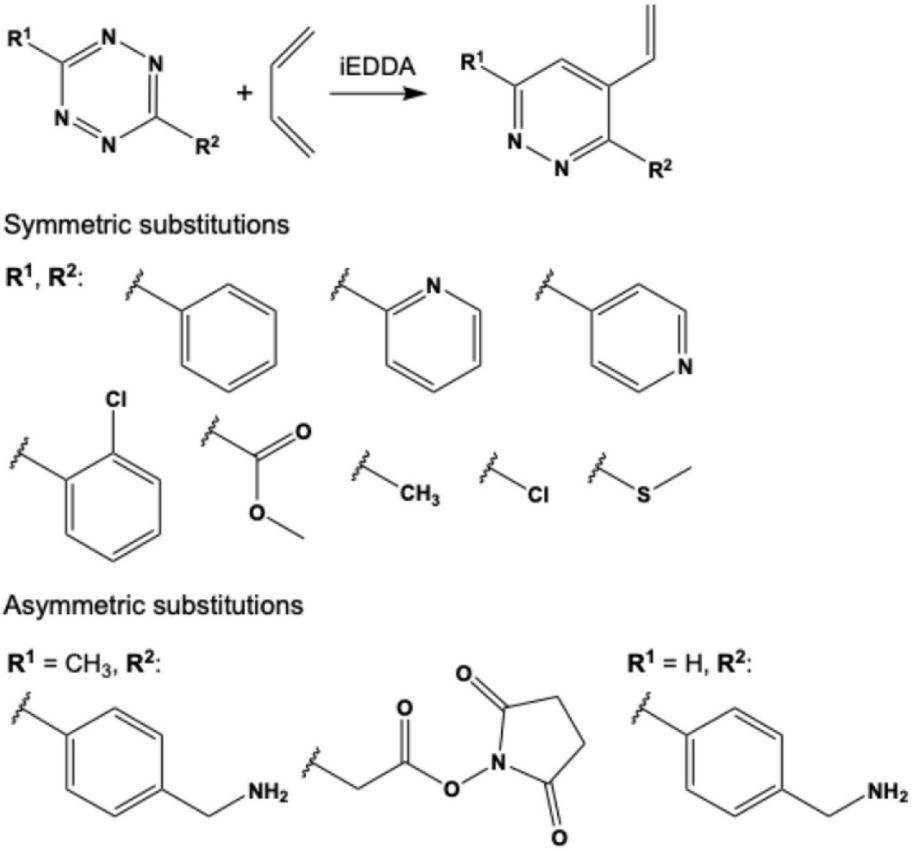

Scheme 1. Expected inverse electron demand Diels–Alder (iEDDA) reaction between 1,3-butadiene and the selected 1,2,4,5-tetrazine derivatives.

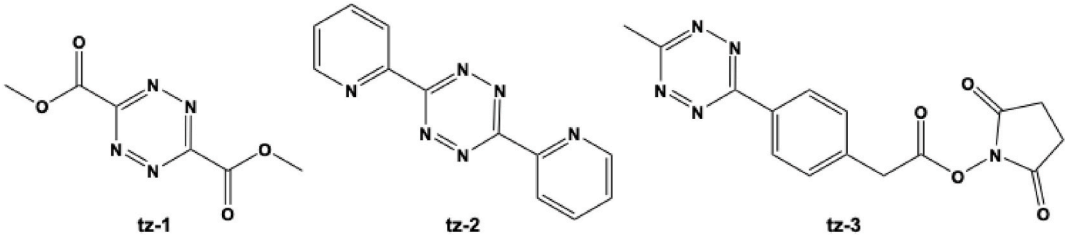

Fig. 1. Tetrazine derivatives whose absorption or emission spectra evolved in the presence of 1,3-butadiene.

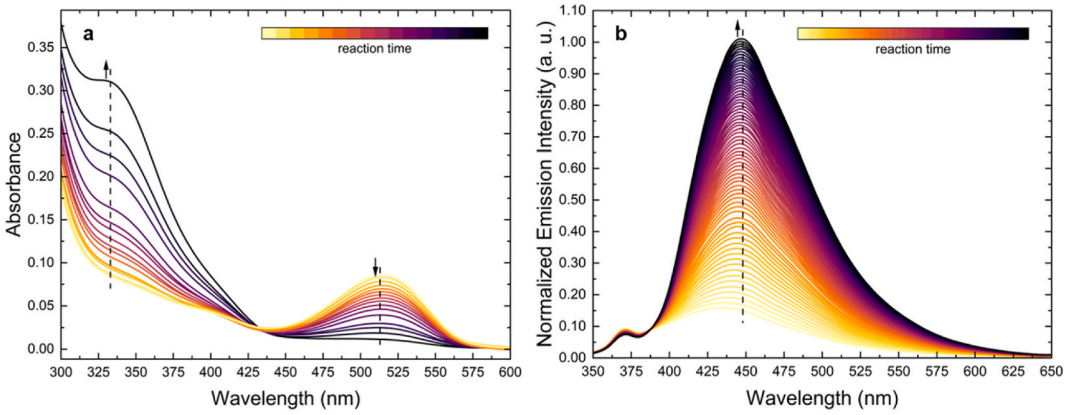

Fig. 2. 2-Hour time evolution of the absorption (a) and emission (λ_{exc} = 333 nm) (b) spectra during the unstirred reaction of **tz-1** (0.24 mM) with excess 1,3-butadiene. Reaction times increase from the yellow to the black spectra, starting at 5 min after addition. (For interpretation of the references to color in this figure legend, the reader is referred to the Web version of this article.)

even more so of its putative $S_1 \rightarrow S_0$ emission energy – which we did not detect – ensuring that the new emission band was not contaminated by the **tz-1** emission. Overall, the almost-immediate production of an off-on emission band upon exposure to 1,3-butadiene made **tz-1** an ideal sensor for the diene, whose detection mechanism and detection merits we explored further.

3.2. Reaction and fluorescence mechanisms

To confirm that **tz-1** reacted with 1,3-butadiene through the inverse electron demand Diels–Alder [4 + 2] cycloaddition, we analyzed the reaction products by nuclear magnetic resonance (NMR). For that, we reacted **tz-1** at 13 mM with excess 1,3-butadiene at room temperature. The starting tetrazine was consumed in less than 15 min, as evaluated through thin layer chromatography and confirmed by ^{1}H NMR analysis of the pre-purification reaction mixture. Performing the reaction under air or inert atmospheres did not influence the NMR spectra of its products, demonstrating it was not sensitive to the atmospheric oxygen. Quick purifications through alumina column chromatography – in a glass Pasteur pipette and eluting with dichloromethane – did not significantly influence the NMR spectrum either, underlining a high reaction product selectivity.

The two ^{1}H NMR singlet peaks found at δ 8.47 ppm and δ 8.31 ppm (Fig. S9), characteristic of nitrogen-bound protons, signaled that the reaction had not progressed towards the expected 3,6-bis(methoxycarbonyl)-4-vinylpyridazine (**pyr**, Scheme 2). Nevertheless, we could find two doublet of doublets (dd) peaks at δ 5.19 ppm and δ 5.08 ppm with coupling constants consistent with geminal coupling between themselves (J = 2.4 Hz) and vinylic *cis* (J = 10.0 Hz) and vinylic *trans* (J = 17.2 Hz) coupling with the doublet of quartets (dq) peak at δ 5.77 ppm. This triad – with all three peaks integrating to the same intensity – was consistent with a vinyl substituent in the reaction product, and thus the addition of 1,3-butadiene to **tz-1**. The same vinyl formation was clear in three other peaks – the geminal doublet (d) peaks at δ 5.50 ppm and δ 5.41 ppm, and the doublet of doublets (dd) peak at δ 7.61 – all sharing the same intensity, albeit 0.15 lower than that of the previous three peaks. That same ratio was calculated from the intensities of the nitrogen-bound protons. These observations led us to consider that the reaction had stopped in one reaction intermediate, rather than having progressed in a different reaction pathway. The nitrogen-bound protons

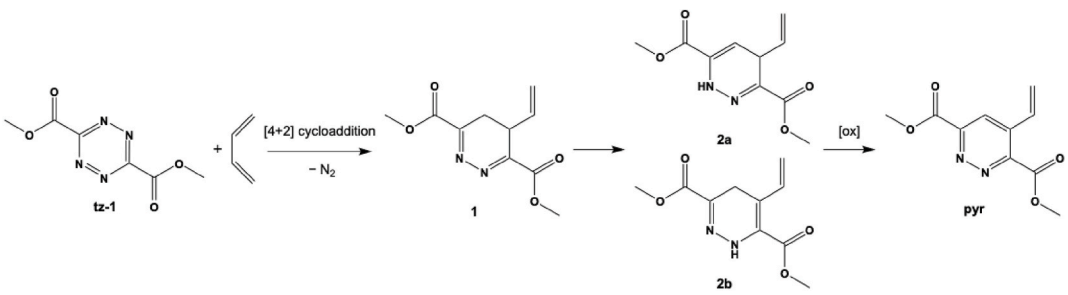

Scheme 2. Inverse electron demand Diels–Alder reaction between **tz-1** and 1,3-butadiene including its 4,5-dihydropyridazine (**1**) and 1,4-dihydropyridazine (**2a** and **2b**) intermediates. The pyridazine product (**pyr**) was not produced.

excluded the 4,5-dihydropyridazine intermediate (**1**) as the reaction product, suggesting instead the 1,4-dihydropyridazine intermediate tautomers **2a** and **2b**. Indeed, the presence of the two tautomers **2** at the 1:0.15 (or 87:13) ratio predicts and explains all other peaks obtained in 1D ^{1}H and ^{13}C and 2D HSQC NMR experiments, as assigned in section S4.

Our results are consistent with previous works on the inverse electron demand Diels–Alder [4 + 2] cycloaddition of 1,2,4,5-tetrazines to dienophiles, as reviewed by Knall et al. [47] and Oliveira et al. [53]. After the addition of a 1,2,4,5-tetrazine to an electron-rich alkene or alkyne to form a highly strained bicyclic intermediate, the latter is rapidly converted to a 4,5-dihydropyridazine derivative (**1**) through a N_2-releasing retro-Diels–Alder reaction. The 4,5-dihydropyridazine (**1**) quickly isomerizes to 1,4-dihydropyridazine tautomers (**2a** and **2b**). At room temperature, the 1,4-dihydropyridazine derivatives are only oxidized to the pyridazine product (**pyr**) in the presence of strong oxidizing agents, such as 2,3-dichloro-5,6-dicyanobenzoquinone (DDQ) [54,55], nitrous gases, isoamyl nitrite, or hydrogen peroxide [47,56]. Thus, in the absence of strong oxidants, the products of the iEDDA reaction between **tz-1** and 1,3-butadiene are expected to be the 1,4-dihydropyridazine tautomers **2a** and **2b**, as we inferred through NMR, and whose emission at 449 nm signals the presence of 1,3-butadiene.

The exceptionally high Stokes shift observed in the photophysical experiments indicates that the 1,4-dihydropyridazines' sensing fluorescence originates from an intramolecular charge-transfer transition. This behavior is consistent with that reported for other dihydropyridazine derivatives [57,58], which typically display Stokes shifts higher than 100 nm [57,59–61]. In compounds **2a** and **2b**, a push-pull charge--transfer system is established by the reduced dihydropyridazine nitrogen (N–H), acting as the electron donor, and the methoxycarbonyl substituent, acting as the electron acceptor, with the two groups connected through the π-system of the pyridazine skeleton.

3.3. Chemoselectivity

Based on frontier molecular orbital theory, the iEDDA reaction rate is optimized by minimizing the difference between the highest occupied molecular orbital (HOMO) of the dienophile (e.g., 1,3-butadiene) and the lowest unoccupied molecular orbital (LUMO) of the diene (e.g., **tz-1**) – ($HOMO_{dienophile} - LUMO_{diene}$) [62]. The **tz-1** indicator shall then react differently with alkene and alkyne dienophiles based on their HOMO energy. We evaluated experimentally if **tz-1** would react with the analytes expectedly present in Titan's lakes, and, if so, whether we could spectroscopically distinguish the reaction product with 1,3-butadiene. For that, we reacted the **tz-1** indicator (at 13.5 mM) with one alkyne (1-pentyne), one terminal alkene (1-hexene), one internal alkene (*cis*-2-hexene), and one cycloalkene (cyclopentene), stable analogues to the simplest and most abundant unsaturated hydrocarbons in Titan's atmosphere – acetylene (C_2H_2), propyne (C_3H_4), diacetylene (C_4H_2), ethylene (C_2H_4), and propene (C_3H_6) [32] – and to the small cyclic molecule cyclopropenylidene (c-C_3H_2) [63]. The competing analytes were reacted at high concentrations (100 mM), and each reaction was timed to 1.5 h.

Evaluated by the **tz-1** absorption at 516 nm, the reaction with 1-pentyne progressed only slightly (Fig. S2a), and significantly less than that with the alkene molecules. A reaction rate higher with olefinic dienophiles than with acetylenic dienophiles has already been noted [64,65] and reasoned from the higher electron withdrawing character of the triple bond [53]. Further, despite some **tz-1** reacted with 1-pentyne, no new emission signal in the spectral region of the 1,3-butadiene products was found (Fig. S2b). This is consistent with the fact that the iEDDA reaction involving alkyne dienophiles directly yields the respective pyridazines, without stabilizing at the 1,4-dihydropyridazine derivatives [53]. This ensures that a **tz-1**-based sensor would not be sensitive to alkyne moieties.

Under the same conditions, the reaction between **tz-1** and all alkenes progressed to completion. The products of all the alkene reactions share similar emission spectra when excited at 333 nm (Fig. 3), suggesting that all tested alkenes reacted with the tetrazine indicator through the same Lindsey-Carboni mechanism towards the formation of the respective 1,4-dihydropyridazine intermediates (Fig. S3). The reaction of **tz-1** with simpler alkenes, likely at significantly higher concentrations than 1,3-butadiene in Titan's lakes, may spend the indicator before it reacts with the intended 1,3-butadiene analyte. This should be addressed in the final application, either by exploring the much lower boiling point (T_B) of the smaller alkenes – T_B (C_2H_4) = −103.7 °C; T_B (C_3H_6) = −47.6 °C – compared to that of 1,3-butadiene – T_B (C_4H_6) = −4.4 °C –, or by immobilizing **tz-1** with catalysts which increase the reaction chemoselectivity towards 1,3-butadiene [66–69].

Given the lack of chemoselectivity of the **tz-1** iEDDA reaction, it is crucial to distinguish the emission signal of the 1,3-butadiene reaction products. We started by investigating the fluorescence lifetimes of the four alkene reaction products. Their analysis through time-correlated single-photon counting (TCSPC) (Fig. S4) showed that the lifetimes of the 2-hexene (τ_{ave} = 591 ± 91 ps) and cyclopentene (τ_{ave} = 519 ± 122 ps) reaction products were not distinguishable from that of the 1,3-butadiene reaction products (τ_{ave} = 590 ± 115 ps) (Table 1), which precludes a spectroscopic selectivity of the latter based on fluorescence lifetimes. The three fluorescence lifetimes were modeled with a two-exponential decay, whereas that of the 1-hexene reaction product was modeled with a single-exponential decay with a significantly higher lifetime (τ = 1296 ± 2). 1-Hexene was thus the only alkene analyte distinguishable by its fluorescence lifetime after reaction with **tz-1** (Fig. 4).

We can, nevertheless, still distinguish the 1,3-butadiene reaction products. As the latter is a conjugated diene, the electron delocalization of the **2b** tautomer is greater than that of the respective 1-hexene, 2-hexene, and cyclopentene reaction product – compare molecules **2b** and **3–5b**, Fig. S3. The conjugation of 1,3-butadiene shall thus explain the extended absorption of its reaction products at 400–440 nm, absent from the absorption spectra of the remaining reaction products (Fig. 5a). The same band is recovered in the **tz-1** + 1,3-butadiene excitation spectrum (Fig. S1) and explains the pale-yellow coloration of the 1,3-butadiene reaction product compared with that of the other alkenes (Fig. 5b).

Exciting the reaction products at different wavelengths along this distinctive shoulder band (415–430 nm, Fig. 6) allows us to distinguish the reaction with 1,3-butadiene. The excitation at 415 nm affords a large emission selectivity, which progressively increases with the excitation at

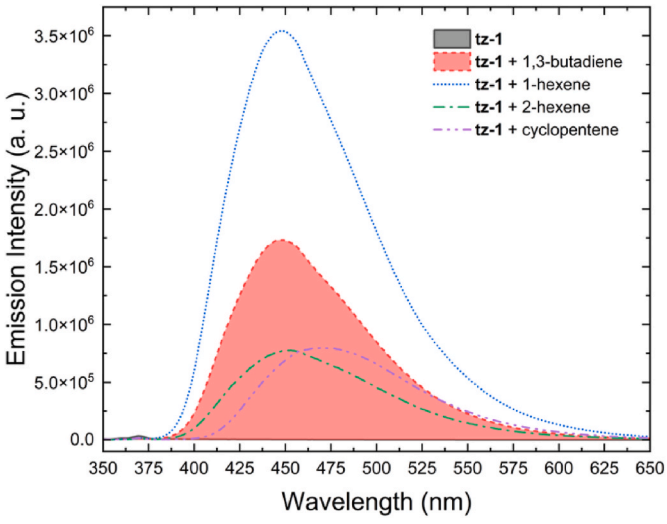

Fig. 3. Emission spectra (λ_{exc} = 333 nm) of the reaction products between **tz-1** and 1,3-butadiene, 1-hexene, *cis*-2-hexene, and cyclopentene. The reactions took place at the same conditions.

Table 1
Fluorescence lifetime components of the reaction products of **tz-1** with the different alkenes.

Component lifetime (ps, ± *SE*)	Component amplitude (±*SE*)	
	Amplitude (A_i, ± *SE*)	Normalized amplitude (α_i)
tz-1 + 1,3-butadiene		
$\tau_1 = 768 \pm 12$	$A_1 = 9462 \pm 399$	38.7 ± 2.7 %
$\tau_2 = 266 \pm 13$	$A_2 = 14991 \pm 266$	61.3 ± 2.7 %
$\tau_{int} = 460 \pm 41$ ps		
$\tau_{amp} = 590 \pm 115$ ps		
tz-1 + 1-hexene		
$\tau_1 = 1296 \pm 2$	$A_1 = 7932 \pm 10$	100 %
tz-1 + 2-hexene		
$\tau_1 = 1063 \pm 16$	$A_1 = 2449 \pm 60$	13.1 ± 0.6 %
$\tau_2 = 187 \pm 6$	$A_2 = 16280 \pm 376$	86.9 ± 4.0 %
$\tau_{int} = 302 \pm 21$ ps		
$\tau_{amp} = 591 \pm 91$ ps		
tz-1 + cyclopentene		
$\tau_1 = 745 \pm 17$	$A_1 = 4814 \pm 308$	28.5 ± 2.6 %
$\tau_2 = 272 \pm 11$	$A_2 = 12095 \pm 180$	71.5 ± 3.1 %
$\tau_{int} = 407 \pm 41$ ps		
$\tau_{amp} = 519 \pm 122$ ps		

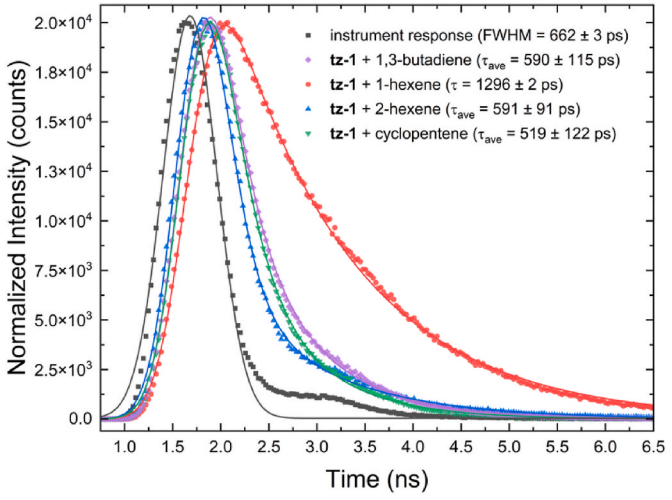

Fig. 4. Normalized fluorescence decay of the reaction products of **tz-1** with different alkenes. Reported average lifetimes were amplitude-averaged as described in section 2.4.

lower energies, to the point that by exciting at 430 nm the emission of the alternative reaction products are not distinguishable from the blank signal (unreacted **tz-1**), whose emission intensity at 449 nm was 66-fold lower than that of the 1,3-butadiene reaction products (Fig. 6). In summary, by probing the reaction mixture at higher wavelengths we can selectively excite the reaction product with 1,3-butadiene; this selectivity arises from the conjugation in the 1,3-butadiene which made it a standout analyte in the first place.

3.4. Limit of detection and response curve

Although the detection figures of merit of the final fiber optic sensor will largely depend on the implemented electronics, we intended to calculate the LOD of this sensing strategy in solution, employing our benchtop equipment. For that we reacted, for 24 h, **tz-1** at 10 mM with different concentrations of 1,3-butadiene ranging from blank (0 μM) to 500 μM, as described in section 2.5. The upper concentration, 500 μM, is higher in molar fraction units – 26 ppm (mol mol^{-1}), using $\rho_{acetonitrile}$ = 786 g l^{-1} at 25 °C – than that of the saturation concentration (c_{sat}) of benzene in Titan's lakes – 11.3 ± 0.9 ppm (mol mol^{-1}), using $c_{sat} = 2.4 (\pm 0.2) \times 10^{-4}$ M [70] and $\rho_{ethane} = 641.2$ g l^{-1} (100 K, 0.10 MPa) [71] –, which we assumed to be the same for 1,3-butadiene. We thus expect the selected range to include all concentrations of 1,3-butadiene possibly found in the lakes of Titan.

At our conditions and equipment, we calculated a tentative LOD of 21 ± 2 μM in acetonitrile, equivalent to 1.1 ± 0.1 ppm (mol mol^{-1}). This LOD would represent a 100-fold improvement to the expected limit of detection of aliphatic organics with SHERLOC (100 ppm [72]). Furthermore, the response curve remained linear up to 500 μM (R^2 = 0.986) (Fig. 7), ensuring a sensor dynamic range which encompasses all expected 1,3-butadiene *in-situ* concentrations.

3.5. Temperature dependence

One appealing advantage of fiber optic chemical sensors is their ability to probe the environment directly, without collecting or treating the environmental samples. The biggest hurdle to such seamless environment investigation on Titan regards its low surface temperature – averaged at 94 K (−179 °C) –, and how little kinetic energy (RT = 0.19 kcal mol^{-1}, where R is the ideal gas constant) it provides to enable thermally activated reactions such as iEDDA, whose activation barriers may be only as low as 3.0 kcal mol^{-1} [73]. To inform a future implementation about operational temperature requirements, we evaluated the temperature dependence of the sensing reaction. We did so by performing the reaction under agitation in 1-cm pathlength quartz cuvettes, whilst continuously monitoring the emission at 449 nm (λ_{exc} = 333 nm). Through a glass syringe we would add 115 μl of an 18.3 mM 1,3-butadiene solution to the quartz cuvette with the **tz-1** indicator solution, allowing afterwards 1,3-butadiene (0.7 mM) to react with **tz-1** (0.24 mM) for up to 9 h. These diluted concentrations ensured that the absorption at the excitation wavelength was not higher than A = 0.1 even when the reaction was complete.

We investigated a short, and mild, range of temperatures from 15 to 35 °C (Fig. 8a). It was, nevertheless, sufficient to demonstrate the high sensitivity of the reaction rate to temperature: during the first 15 min of reaction (allowing 5 min to homogenize) the reaction rate at 35 °C was 1 order of magnitude faster than that at 15 °C, suggesting that a **tz-1**-based sensor for 1,3-butadiene should highly benefit from a heated environment. For it to directly probe Titan's surface, heating elements could be coupled to the environment-interacting tip. Alternatively, the FOCS could be integrated with other instruments which acquire the samples to the spacecraft interior. Hypothetically, the integration in the gas phase inlet of Dragonfly's mass spectrometer [74] would increase the certainty in putative assignments of mass spectral peaks to 1,3-butadiene.

At 15 °C – and at such diluted concentrations – 19 s of reaction were enough to accumulate signal above 10 times the y-intercept standard error of a linear fit of the early time evolution (Fig. 8a), demonstrating the low operational timeframes that would be required from a **tz-1**-based sensor.

Although the temperature dependence was clear, the reaction rates showed significant variability for any given temperature (not shown), for which reason we lacked confidence to calculate the activation energy of this reaction in solution. The observed variability likely resides in the manipulation and addition of 1,3-butadiene to the quartz cuvette. Not only its manual addition through a glass syringe may produce momentaneous, yet impactful, heterogeneities in the reacting solution, but also the low boiling point of 1,3-butadiene (−4.4 °C) made it difficult to stabilize the analyte in solution and be confident about its concentration reproducibility between experiments. The same concerns apply to the calibration curve above (Fig. 7). Furthermore, irradiating the reaction product after the reaction was complete, we understood that the continuous irradiation of the reaction mixture was consuming the fluorescent reaction product. We attribute this consumption to the photooxidation reaction of the 1,4-dihydropyridazines **2**, as residually formed pyridazines may act as photosensitizers to produce singlet

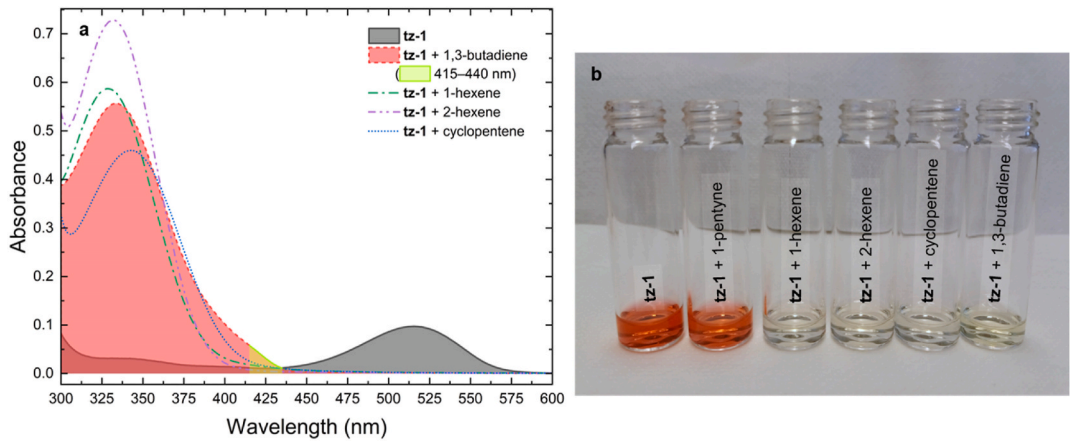

Fig. 5. Absorption spectra (a) and photographs (b) of the reaction products between the tetrazine indicator (**tz-1**) and the different alkenes. a. Within the 415–440 nm region of the absorption spectrum (yellow), the 1,3-butadiene reaction product is distinguishable from that of the other alkenes. b. The reaction with 1-pentyne retained the same color as the unreacted, blank, tetrazine solution; the color of the reaction products with 1,3-butadiene (pale-yellow) differed from that with the remaining alkenes (almost colorless). (For interpretation of the references to color in this figure legend, the reader is referred to the Web version of this article.)

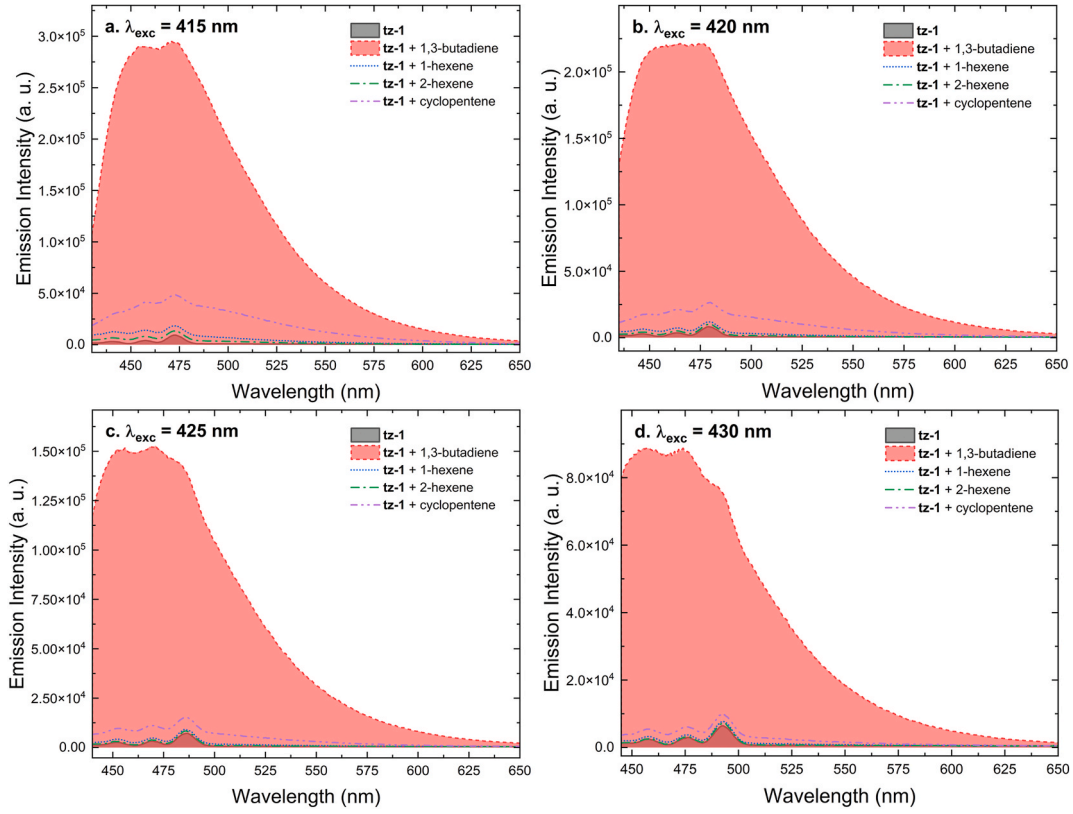

Fig. 6. Emission spectra of the reaction products of the tetrazine indicator **tz-1** with different alkenes whilst exciting at 415 nm (a), 420 nm (b), 425 nm (c), and 430 nm (d).

oxygen capable of oxidizing the 1,4-dihydropyridazines derivatives [56]. Such photooxidation would be mitigated in the anoxic environment of Titan, albeit UV irradiation under anoxic conditions similarly photochemically transforms the 1,4-dihydropyridazines into the pyridazine, this time through a disproportionation pathway [56] (Scheme S1).

To decrease the rate of product consumption relative to the rate of product formation – and thus mitigate the influence of the product photoreaction – we should perform these measurements at high temperatures. Contrary to the reaction itself (Fig. 8a), the photochemical transformation of the emitting product does not depend on temperature, having shown constant disappearance rates upon irradiation from 35 °C down to 15 °C (Fig. 8b), as is proper of photochemical reactions. The best reaction product preservation strategy would be, however, to excite the membrane – to interrogate its emission intensity – as sporadically as possible, and to combine it with low intensity light emission diodes (LED) as excitation sources, instead of the high intensity (450-W xenon arc) lamps herein employed.

3.6. Solid-state implementation

Lastly, we evaluated whether the **tz-1** indicator can be integrated in

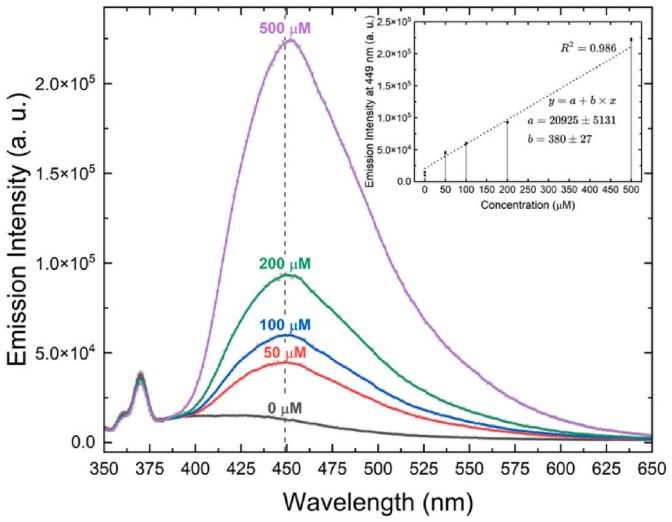

Fig. 7. Emission spectra of the reaction products of **tz-1** with 1,3-butadiene at different concentrations. Inset: calibration curve of the intensity at the emission maximum (449 nm) plotted over the 1,3-butadiene concentration.

an extrinsic fiber optic sensor. For that, we tested the reactivity of **tz-1** immobilized in solid-state substrates. In the process, we were faced with the heavy dependence of Diels–Alder reactions on the reactants' spatial orientation and proximity of the reacting π systems. With the **tz-1** indicator immobilized in the solid state, where the mobility of molecules is significantly reduced compared to that in solution, there are fewer opportunities for the concerted pericyclic reaction to occur, making the latter kinetically hindered compared to its solution-phase counterpart. On the contrary, solid-state films can immobilize a very high number of indicator molecules per unit volume – in the experiments described below we immobilized ~1.2 mg (6.1 μmol) of **tz-1** in 1 × 4 cm^2 thin films –, effectively increasing the concentration of reacting indicators. Furthermore, the reaction solvent may affect dramatically the reaction rate of iEDDA, with hydrophobic solvents capable of slowing the reaction rates down by two orders of magnitude compared to aqueous solutions [40,75]. To account for such solvent dependency, we evaluated the reactivity of the immobilized **tz-1** with 1,3-butadiene in hexane, a solvent analogous to Titan's lakes.

As introduced, the hydrocarbon lakes of Titan are highly apolar, with relative dielectric constants on the order of $\varepsilon_r = 1.5–2$ [76] (compare to water's $\varepsilon_r = 80$ at 20 °C), explained by a composition dominated by methane and ethane [28]. They constitute 1.5 % of Titan's surface [77], making it the only extraterrestrial world in the Solar System with surface liquid bodies. The lakes are overlain by an atmosphere of roughly 95 % nitrogen and 5 % methane which produces a surface pressure of approximately 1.5 bar [78], in close resemblance to Earth's surface. Contrastingly though, Titan's surface is anoxic and thermally inert (on average at −179 °C), it lacks any liquid water, and its solar irradiance is only 0.1 % of that incident on Earth's surface [79], depleted of its UV component [80]. Overall, Titan's lakes exist in an Earth-like environment without its main physicochemical stressors. Having tested the operation of the immobilized indicator in hexane ($\varepsilon_r = 1.9$ at 20 °C) at Earth's room atmosphere and temperature, we imposed in it harsher conditions than those it may face in the final application.

For our intended application, an appropriate solid-state substrate should be insoluble in hydrocarbon solvents, simultaneously prevent the lixiviation of the **tz-1** indicator and the reaction products, whilst permitting the diffusion of 1,3-butadiene towards the immobilized **tz-1**. We only evaluated polymeric membranes as possible substrates. The most robust of which, addressing all previous requirements, was polyurethane-based, produced from curing a poly(hexamethylenediisocyanate) pre-polymer with trimethylolpropane [81]. We successfully immobilized **tz-3** in a polyurethane membrane and measured the formation of an emission band signaling its reaction with 1,3-butadiene. **Tz-1**, however, degraded during the polyurethane curing process – by a likely reaction with the isocyanate groups [82]. Alternatively, polystyrene was considered, owing to its lower solubility in alkanes of lower molecular weight [83]; not only is it insoluble in hexane [84] but it should be much more so in the methane/ethane lakes of Titan. Polystyrene films adhered to Mylar® sheets proved to be suitable substrates for **tz-1**.

We then evaluated the reactivity of the **tz-1** polystyrene film with 1,3-butadiene. We immersed the film in a hexane solution with 1,3-butadiene (18 mM) at room temperature and under continuous stirring (Fig. S5). After 15 h we observed the complete color evolution detected in solution – from a red to a pale-yellow coloration – without any loss in film homogeneity and structural integrity (Fig. 9a). The absorption and emission spectra (λ_{exc} = 333 nm) evolved similarly to their solution counterparts – albeit the new emission maximum blue-shifted to 425 nm (Fig. 9b). Such blue shift can be attributed to the lower polarity of the polystyrene membrane compared with that of acetonitrile. Because it is less polar, the polystyrene environment stabilizes less effectively the excited-state dipole formed after the intramolecular charge-transfer transition (section 3.2). As a result, the LUMO of the fluorescent product remains at a higher energy, leading to the emission of higher-energy (blue-shifted) photons.

These experiments demonstrated that the sensing reaction is possible in solid-state and in hydrophobic solvents as those expected on Titan, having also shown that polystyrene polymeric membranes are viable immobilizing substrates going forward. Studying the emission of the empty Mylar® sheet and that of an empty polystyrene film adhered to

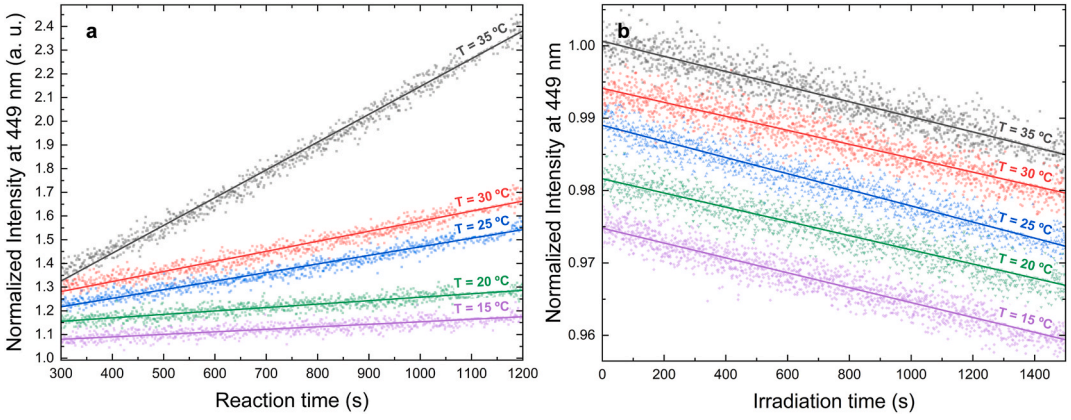

Fig. 8. Early time evolution of the emission intensity at 449 nm (λ_{exc} = 333 nm) of the reaction between **tz-1** and 1,3-butadiene (a) and product consumption during irradiation (λ_{exc} = 333 nm) (b) at varying temperatures. All data were normalized to the emission at t = 0 s and shifted vertically for clarity.

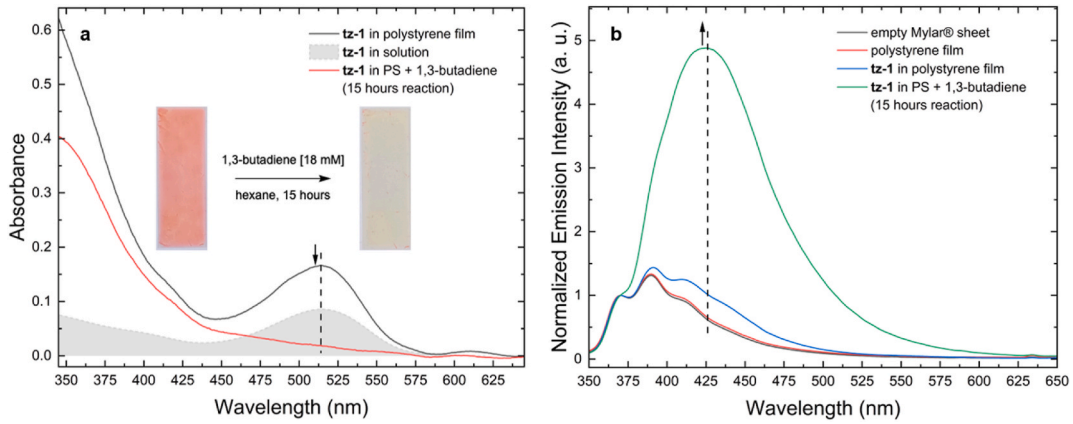

Fig. 9. Absorption (a) and emission (λ_{exc} = 333 nm) (b) spectra of **tz-1** immobilized in a polystyrene film before and after exposure to 1,3-butadiene. The absorption spectra of **tz-1** in solution (a) and the emission spectra of an empty Mylar® sheet and a polystyrene film (b) were added for comparison. The emission intensities of each spectrum were normalized to those at 370 nm.

the Mylar® sheet, we understood that the Mylar® sheet produced a significant background signal (Fig. 9b). Although it did not mask the new emission band after the exposure to 1,3-butadiene, its removal altogether may be desirable. To do so, future solid-state implementations should consider fabricating the polystyrene films on quartz slides, rather than Mylar® sheets.

4. Conclusions and future work

In this work we describe the discovery and characterization of the first fluorescence-based indicator for 1,3-butadiene. A long screening led us to select 3,6-bis(methoxycarbonyl)-1,2,4,5-tetrazine (**tz-1**) as the best candidate. By NMR we confirmed that the two molecules reacted through an iEDDA click-reaction, promoting the selective, remarkably fast, and irreversible formation of emissive 1,4-dihydropyridazine derivatives. Despite the lack of reaction chemoselectivity against other alkene reactants, we can infer the reaction with 1,3-butadiene through the distinct absorption of its 1,4-dihydropyridazine product **2b**. By exciting the reaction products at wavelengths higher than 415 nm we obtain emission signals selective to 1,3-butadiene (Fig. 6). Performed *in-situ*, this selectivity towards 1,3-butadiene can guide and complement the results from more complex spectrofluorometers or mass spectrometers.

The sensor response curve obtained in solution suggests that future implementations may detect 1,3-butadiene concentrations as low as 1.1 ppm (mol mol^{-1}) and up to the expected saturation concentration in Titan's lakes. Also, the fast click-reaction with 1,3-butadiene shall lead to quick sensor responses, which increase significantly with temperature. High-temperature implementations would both volatilize the smaller competing alkenes expected on Titan – minimizing their interaction with the sensing membrane – and ensure that the formation of the emissive 1,4-dihydropyridazines out-weights subsequent photochemical reactions initiated by the excitation source. To further minimize the reaction product consumption, the responsive membrane should be probed with low intensity LED and at high time increments (e.g., 20 s). Upon immobilization in a polystyrene film, the **tz-1** indicator reacted with 1,3-butadiene in a hexane solution, having demonstrated the same spectroscopic evolution inferred from dissolved **tz-1**. The solid-state implementation represents a crucial validation before its integration with space-ready instrumentation, whose final solid-state immobilization will be tailored accordingly. We intend to explore the diversity of tetrazine functionalization strategies [68] to increase the reaction rate with the immobilized **tz-1**, as well as combine the latter with catalysts which increase the chemoselectivity towards 1,3-butadiene [66–69].

Overall, we have reported on our ongoing efforts to build FOCS prepared for extraterrestrial chemical detections. We expect that this proof-of-concept 1,3-butadiene sensing strategy motivates further researchers to contribute to space exploration through the towering knowledge on fluorescence sensing. It is our belief that FOCS can complement the *in-situ* detection of organic molecules in space applications, given their easy miniaturization and high flexibility, combined with notable ruggedness and resilience to electromagnetic interference. Acting as low power semiquantitative complements to more capable instruments, they may produce high scientific value, or calibration means, at low costs. The chemosensing field can build on the success of previous *in-situ* characterization instruments and complement those of the future [15].

CRediT authorship contribution statement

Diogo Gonçalves: Writing – review & editing, Writing – original draft, Investigation, Funding acquisition, Formal analysis, Data curation, Conceptualization. **Cláudia Ribeiro:** Writing – review & editing, Investigation. **João P.C. Tomé:** Writing – review & editing, Validation, Supervision, Resources, Formal analysis. **Bruno Pedras:** Writing – review & editing, Validation, Supervision, Resources, Funding acquisition, Conceptualization. **Zita Martins:** Writing – review & editing, Validation, Supervision, Resources, Project administration, Funding acquisition, Conceptualization.

Declaration of competing interest

The authors declare that they have no known competing financial interests or personal relationships that could have appeared to influence the work reported in this paper.

Acknowledgments

Centro de Química Estrutural acknowledges the financial support of Fundação para a Ciência e Tecnologia (FCT) through projects UIDB/00100/2020 and UIDP/00100/2020. Institute of Molecular Sciences acknowledges the financial support of FCT through project LA/P/0056/2020. Institute for Bioengineering and Biosciences acknowledges the financial support of FCT through projects UIDB/04565/2020 and UIDP/04565/2020. The Associate Laboratory Institute for Health and Bioeconomy (i4HB) acknowledges the financial support of FCT through project LA/P/0140/2020. DG acknowledges the financial support of FCT through grant 2021.04932.BD. CR acknowledges the financial support from FCT through grant UI/BD/152798/2022.

Appendix A. Supplementary data

Supplementary data to this article can be found online at https://doi.org/10.1016/j.aca.2025.344982.

Data availability

Data will be made available on request.

References

[1] C. Pendão, I. Silva, Optical Fiber sensors and sensing networks: overview of the main principles and applications, Sensors 22 (2022) 7554, https://doi.org/10.3390/S22197554.

[2] N. Sabri, S.A. Aljunid, M.S. Salim, S. Fouad, Fiber optic sensors: short review and applications, in: Recent Trends in Physics of Material Science and Technology. Springer Series in Materials Science, Springer, Singapore, 2015, pp. 299–311, https://doi.org/10.1007/978-981-287-128-2_19.

[3] D. Tosi, S. Poeggel, I. Iordachita, E. Schena, Fiber optic sensors for biomedical applications, in: Opto-Mechanical Fiber Optic Sensors: Research, Technology, and Applications in Mechanical Sensing, Butterworth-Heinemann, 2018, pp. 301–333, https://doi.org/10.1016/B978-0-12-803131-5.00011-8.

[4] M. Elsherif, A.E. Salih, M.G. Muñoz, F. Alam, B. AlQattan, D.S. Antonysamy, M. F. Zaki, A.K. Yetisen, S. Park, T.D. Wilkinson, H. Butt, Optical Fiber sensors: working principle, applications, and limitations, Adv Photonics Res 3 (2022) 2100371, https://doi.org/10.1002/ADPR.202100371.

[5] I. McKenzie, S. Ibrahim, E. Haddad, S. Abad, A. Hurni, L.K. Cheng, Fiber optic sensing in spacecraft engineering: an historical perspective from the European Space Agency, Front. Phys. 9 (2021) 719441, https://doi.org/10.3389/FPHY.2021.719441.

[6] A. Riva, M. Gai, M.G. Lattanzi, F. Russo, R. Buzzi, A. Riva, M. Gai, M.G. Lattanzi, F. Russo, R. Buzzi, BAM: a metrology device for a high precision astrometric mission, in: J.C. Tello, A. Riva, D. Hiriart, A.J. Castro-Tirado (Eds.), III Workshop on Robotic Autonomous Observatories, Revista Mexicana De Astronomía Y Astrofísica, Serie de Conferencias), 2013, p. 38.

[7] I. Jernej, M. Faust, R. Lammegger, I. McKenzie, J. Kuhnhenn, C. Knothe, S. O'Riorden, J. Barbero, P. Brown, V. Lelievre, M. Agú, A. Alessi, C. Amtmann, A. Betzler, M. Dougherty, M. Ellmeier, C. Hagen, A. Hauser, M. Hartig, A. Lamott, M. Leichtfried, W. Magnes, A. Mahapatra, S. Mariojouls, D. Monteiro, A. Pollinger, A. Salomon, U. Weinand, R. Wolf, Design and test of the optical fiber assemblies for the scalar magnetic field sensor aboard the JUICE mission, in: Proceedings Volume 11852, International Conference on Space Optics — ICSO 2020, SPIE, 2021, pp. 2487–2501, https://doi.org/10.1117/12.2600052.

[8] X.D. Wang, O.S. Wolfbeis, Fiber-optic chemical sensors and biosensors (2015-2019), Anal. Chem. 92 (2020) 397–430, https://doi.org/10.1021/ACS.ANALCHEM.9B04708.

[9] C. McDonagh, C.S. Burke, B.D. MacCraith, Optical chemical sensors, Chem. Rev. 108 (2008) 400–422, https://doi.org/10.1021/CR068102G.

[10] T.H. Nguyen, T. Sun, Optical fibre chemical sensors, in: Optical Fibre Sensors, John Wiley & Sons, Ltd, 2020, pp. 239–288, https://doi.org/10.1002/9781119534730.CH8.

[11] W.R. Seitz, M.J. Sepaniak, Chemical sensors based on immobilized indicators and fiber optics, CRC Crit. Rev. Anal. Chem. 19 (1988) 135–173, https://doi.org/10.1080/10408348808542810.

[12] M. Pospíšilová, G. Kuncová, J. Trögl, Fiber-Optic chemical sensors and fiber-optic bio-sensors, Sensors 15 (2015) 25259, https://doi.org/10.3390/S151025208.

[13] K.M. Seaton, M.L. Cable, A.M. Stockton, Analytical chemistry in astrobiology, Anal. Chem. 93 (2021) 5981–5997, https://doi.org/10.1021/ACS.ANALCHEM.0C04271.

[14] K.M. Seaton, M.L. Cable, A.M. Stockton, Analytical chemistry throughout this solar System, Annu. Rev. Anal. Chem. 15 (2022) 197–219, https://doi.org/10.1146/ANNUREV-ANCHEM-061020-125416.

[15] V. Abrahamsson, I. Kanik, In situ organic biosignature detection techniques for space applications, Frontiers in Astronomy and Space Sciences 9 (2022) 959670, https://doi.org/10.3389/FSPAS.2022.959670.

[16] S. Gao, X. Yang, S. Wang, C. Chu, P. Teng, F. Tian, Y. Zhang, Z. Liu, X. Yang, Review of optical fiber optofluidic chemical sensors and biosensors, Photonic Sensors 15 (2024) 1–36, https://doi.org/10.1007/S13320-024-0710-8.

[17] X. Lu, P.J. Thomas, J.O. Hellevang, A review of methods for fibre-optic distributed chemical sensing, Sensors 19 (2019) 2876, https://doi.org/10.3390/S19132876.

[18] M. jie Yin, B. Gu, Q.F. An, C. Yang, Y.L. Guan, K.T. Yong, Recent development of fiber-optic chemical sensors and biosensors: mechanisms, materials, micro/nano-fabrications and applications, Coord. Chem. Rev. 376 (2018) 348–392, https://doi.org/10.1016/J.CCR.2018.08.001.

[19] B. Valeur, M.N. Berberan-Santos, Chemical sensing via fluorescence, in: Molecular Fluorescence, second ed., John Wiley & Sons, Ltd, 2012, pp. 409–478, https://doi.org/10.1002/9783527650002.CH14.

[20] R. Miao, J. Peng, Y. Fang, Recent advances in fluorescent film sensing from the perspective of both molecular design and film engineering, Mol Syst Des Eng 1 (2016) 242–257, https://doi.org/10.1039/C6ME00039H.

[21] O.S. Wolfbeis, Luminescent sensing and imaging of oxygen: fierce competition to the Clark electrode, Bioessays 37 (2015) 921–928, https://doi.org/10.1002/BIES.201500002.

[22] L. Ding, Y. Fang, Chemically assembled monolayers of fluorophores as chemical sensing materials, Chem. Soc. Rev. 39 (2010) 4258–4273, https://doi.org/10.1039/C003028G.

[23] R. Bhartia, L.W. Beegle, L. DeFlores, W. Abbey, J. Razzell Hollis, K. Uckert, B. Monacelli, K.S. Edgett, M.R. Kennedy, M. Sylvia, D. Aldrich, M. Anderson, S. A. Asher, Z. Bailey, K. Boyd, A.S. Burton, M. Caffrey, M.J. Calaway, R. Calvet, B. Cameron, M.A. Caplinger, B.L. Carrier, N. Chen, A. Chen, M.J. Clark, S. Clegg, P. G. Conrad, M. Cooper, K.N. Davis, B. Ehlmann, L. Facto, M.D. Fries, D.H. Garrison, D. Gasway, F.T. Ghaemi, T.G. Graff, K.P. Hand, C. Harris, J.D. Hein, N. Heinz, H. Herzog, E. Hochberg, A. Houck, W.F. Hug, E.H. Jensen, L.C. Kah, J. Kennedy, R. Krylo, J. Lam, M. Lindeman, J. McGlown, J. Michel, E. Miller, Z. Mills, M. E. Minitti, F. Mok, J. Moore, K.H. Nealson, A. Nelson, R. Newell, B.E. Nixon, D. A. Nordman, D. Nuding, S. Orellana, M. Pauken, G. Peterson, R. Pollock, H. Quinn, C. Quinto, M.A. Ravine, R.D. Reid, J. Riendeau, A.J. Ross, J. Sackos, J.A. Schaffner, M. Schwochert, M. O Shelton, R. Simon, C.L. Smith, P. Sobron, K. Steadman, A. Steele, D. Thiessen, V.D. Tran, T. Tsai, M. Tuite, E. Tung, R. Wehbe, R. Weinberg, R.H. Weiner, R.C. Wiens, K. Williford, C. Wollonciej, Y.H. Wu, R. A. Yingst, J. Zan, Perseverance's scanning habitable environments with raman and luminescence for organics and chemicals (SHERLOC) investigation, Space Sci. Rev. 217 (2021) 1–115, https://doi.org/10.1007/S11214-021-00812-Z.

[24] J. Razzell Hollis, W. Abbey, L.W. Beegle, R. Bhartia, B.L. Ehlmann, J. Miura, B. Monacelli, K. Moore, A. Nordman, E. Scheller, K. Uckert, Y.H. Wu, A deep-ultraviolet Raman and Fluorescence spectral library of 62 minerals for the SHERLOC instrument onboard Mars 2020, Planet. Space Sci. 209 (2021) 105356, https://doi.org/10.1016/J.PSS.2021.105356.

[25] J. Razzell Hollis, S. Sharma, W. Abbey, R. Bhartia, L. Beegle, M. Fries, J.D. Hein, B. Monacelli, A.D. Nordman, A deep ultraviolet raman and Fluorescence Spectral Library of 51 organic compounds for the SHERLOC instrument onboard Mars 2020, Astrobiology 23 (2023) 1–23, https://doi.org/10.1089/AST.2022.0023.

[26] M.J. Malaska, R. Bhartia, K.S. Manatt, J.C. Priscu, W.J. Abbey, B. Mellerowicz, J. Palmowski, G.L. Paulsen, K. Zacny, E.J. Eshelman, J. D'Andrilli, Subsurface in situ detection of microbes and diverse organic matter hotspots in the Greenland ice sheet, Astrobiology 20 (2020) 1185–1211, https://doi.org/10.1089/AST.2020.2241.

[27] D. Cordier, O. Mousis, J.I. Lunine, S. Lebonnois, P. Rannou, P. Lavvas, L.Q. Lobo, A. G.M. Ferreira, Titan's lakes chemical composition: sources of uncertainties and variability, Planet. Space Sci. 61 (2012) 99–107, https://doi.org/10.1016/J.PSS.2011.05.009.

[28] D. Cordier, O. Mousis, J.I. Lunine, P. Lavvas, V. Vuitton, An estimate of the chemical composition of Titan's Lakes, Astrophys. J. 707 (2009) L128, https://doi.org/10.1088/0004-637X/707/2/L128.

[29] D. Cordier, J.W. Barnes, A.G. Ferreira, On the chemical composition of Titan's dry lakebed evaporites, Icarus 226 (2013) 1431–1437, https://doi.org/10.1016/J.ICARUS.2013.07.026.

[30] A.G. Hayes, The Lakes and Seas of Titan, Annu. Rev. Earth Planet Sci. 44 (2016) 57–83, https://doi.org/10.1146/annurev-earth-060115-012247.

[31] V.A. Krasnopolsky, A photochemical model of Titan's atmosphere and ionosphere, Icarus 201 (2009) 226–256, https://doi.org/10.1016/J.ICARUS.2008.12.038.

[32] V. Vuitton, R.V. Yelle, S.J. Klippenstein, S.M. Hörst, P. Lavvas, Simulating the density of organic species in the atmosphere of Titan with a coupled ion-neutral photochemical model, Icarus 324 (2019) 120–197, https://doi.org/10.1016/J.ICARUS.2018.06.013.

[33] T.H. Vu, H.E. Maynard-Casely, M.L. Cable, M. Choukroun, M.J. Malaska, R. Hodyss, 1,3-Butadiene on Titan: crystal structure, thermal expansivity, and raman signatures, ACS Earth Space Chem. 6 (2022) 2274–2281, https://doi.org/10.1021/ACSEARTHSPACECHEM.1C00364.

[34] H.E. Maynard-Casely, M.L. Cable, M.J. Malaska, T.H. Vu, M. Choukroun, R. Hodyss, Prospects for mineralogy on Titan, Am. Mineral. 103 (2018) 343–349, https://doi.org/10.2138/am-2018-6259.

[35] J. Saltiel, D.F. Sears, A.M. Turek, UV spectrum of the high energy conformer of 1,3-Butadiene in the gas phase, J. Phys. Chem. A 105 (2001) 7569–7578, https://doi.org/10.1021/JP011493C.

[36] A. Fahr, A.K. Nayak, Temperature dependent ultraviolet absorption cross sections of 1,3-butadiene and butadiyne, Chem. Phys. 189 (1994) 725–731, https://doi.org/10.1016/0301-0104(94)00306-8.

[37] N.A. Teanby, B. Bézard, S. Vinatier, M. Sylvestre, C.A. Nixon, P.G.J. Irwin, R.J. De Kok, S.B. Calcutt, F. Michael Flasar, The formation and evolution of Titan's winter polar vortex, Nat. Commun. 8 (2017) 1–13, https://doi.org/10.1038/s41467-017-01839-z.

[38] C.A. Nixon, The composition and chemistry of Titan's atmosphere, ACS Earth Space Chem. 8 (2024) 406–456, https://doi.org/10.1021/ACSEARTHSPACECHEM.2C00041.

[39] R.A. Carboni, R.V. Lindsey, Reactions of tetrazines with unsaturated compounds. A new synthesis of pyridazines, J. Am. Chem. Soc. 81 (1959) 4342–4346, https://doi.org/10.1021/JA01525A060.

[40] M.L. Blackman, M. Royzen, J.M. Fox, Tetrazine ligation: fast bioconjugation based on inverse-electron-demand Diels-Alder reactivity, J. Am. Chem. Soc. 130 (2008) 13518–13519, https://doi.org/10.1021/JA8053805.

[41] N.K. Devaraj, R. Weissleder, S.A. Hilderbrand, Tetrazine-based cycloadditions: application to pretargeted live cell imaging, Bioconjug. Chem. 19 (2008) 2297–2299, https://doi.org/10.1021/BC8004446.

[42] M. Pagel, Inverse electron demand Diels–Alder (IEDDA) reactions in peptide chemistry, J. Pept. Sci. 25 (2019) e3141, https://doi.org/10.1002/PSC.3141.

[43] M. Handula, K.-T. Chen, Y. Seimbille, J. Thomas, N. Joseph, D. Eremin, IEDDA: an attractive bioorthogonal reaction for biomedical applications, Molecules 26 (2021), https://doi.org/10.3390/MOLECULES26154640, 4640 26 (2021) 4640.

[44] L. Yan, Z. Zhao, Y. Liu, S.H. Hosseini, C. Li, Y. Huang, M.R. Saeb, H. Xiao, F. Seidi, The inverse electron demand diels-alder (IEDDA): a facile bioorthogonal click reaction for development of injectable polysaccharide-based hydrogels for biomedical applications, Carbohydr. Polym. 352 (2025) 123142, https://doi.org/10.1016/J.CARBPOL.2024.123142.
[45] L.M. Haiber, M. Kufleitner, V. Wittmann, Application of the inverse-electron-demand diels-alder reaction for metabolic glycoengineering, Front. Chem. 9 (2021) 654932, https://doi.org/10.3389/FCHEM.2021.654932.
[46] E. Kozma, O. Demeter, P. Kele, Bio-orthogonal fluorescent labelling of biopolymers through inverse-electron-demand diels–alder reactions, Chembiochem 18 (2017) 486–501, https://doi.org/10.1002/CBIC.201600607.
[47] A.C. Knall, C. Slugovc, Inverse electron demand Diels–Alder (iEDDA)-initiated conjugation: a (high) potential click chemistry scheme, Chem. Soc. Rev. 42 (2013) 5131–5142, https://doi.org/10.1039/C3CS60049A.
[48] S.K. Manna, A. Gangopadhyay, K. Maiti, S. Mondal, A.K. Mahapatra, Recent developments in fluorometric and colorimetric chemodosimeters targeted towards hydrazine sensing: present success and future possibilities, ChemistrySelect 4 (2019) 7219–7245, https://doi.org/10.1002/SLCT.201803685.
[49] A. Maiti, S.K. Manna, D. Banik, A.K. Mahapatra, Name reactions: strategies in the design of chemodosimeters for analyte detection, New J. Chem. 45 (2021) 20046–20074, https://doi.org/10.1039/D1NJ04056A.
[50] S.K. Manna, D. Kuilya, A. Adhikary, A. Maiti, S. Mondal, A minireview of recent developments in ozone detection using optical chemodosimeters, Analyst 148 (2023) 954–965, https://doi.org/10.1039/D2AN01971J.
[51] Y. Yang, Q. Zhao, W. Feng, F. Li, Luminescent chemodosimeters for bioimaging, Chem. Rev. 113 (2013) 192–270, https://doi.org/10.1021/CR2004103.
[52] I. Marr, A. Groß, R. Moos, Overview on conductometric solid-state gas dosimeters, Journal of Sensors and Sensor Systems 3 (2014) 29–46, https://doi.org/10.5194/JSSS-3-29-2014.
[53] B.L. Oliveira, Z. Guo, G.J.L. Bernardes, Inverse electron demand Diels–Alder reactions in chemical biology, Chem. Soc. Rev. 46 (2017) 4895–4950, https://doi.org/10.1039/C7CS00184C.
[54] H. Wu, J. Yang, J. Šečkute, N.K. Devaraj, In situ synthesis of alkenyl tetrazines for highly fluorogenic bioorthogonal live-cell imaging probes, Angew. Chem., Int. Ed. 53 (2014) 5805–5809, https://doi.org/10.1002/ANIE.201400135.
[55] K. Lang, L. Davis, J. Torres-Kolbus, C. Chou, A. Deiters, J.W. Chin, Genetically encoded norbornene directs site-specific cellular protein labelling via a rapid bioorthogonal reaction, Nat. Chem. 4 (2012) 298–304, https://doi.org/10.1038/nchem.1250.
[56] F. Karaki, T. Kiguchi, K. Itoh, N. Sato, K. Konishi, H. Fujii, Catalyst-free photooxidation reaction from 1,4-dihydropyridazine to pyridazine under air, Tetrahedron 97 (2021) 132411, https://doi.org/10.1016/J.TET.2021.132411.
[57] R. Koçak, D. Yıldız, U. Bozkaya, A. Daştan, Ö.A. Bozdemir, Dihydropyridazine-appended dibenzosuberenones as a new class of fluorophores: application to fluoride sensing, Tetrahedron Lett. 58 (2017) 2981–2985, https://doi.org/10.1016/J.TETLET.2017.06.059.
[58] J. Galeta, R. Dzijak, J. Oboril, M. Dračínský, M. Vrabel, A systematic Study of coumarin–tetrazine Light-Up probes for bioorthogonal fluorescence imaging, Chem. Eur J. 26 (2020) 9945–9953, https://doi.org/10.1002/CHEM.202001290.
[59] R. Koçak, A. Dastan, Synthesis of dibenzosuberenone-based novel polycyclic π-conjugated dihydropyridazines, pyridazines and pyrroles, Beilstein J. Org. Chem. 17 (2021) 719–729, https://doi.org/10.3762/BJOC.17.61.
[60] A. Vázquez, R. Dzijak, M. Dračínský, R. Rampmaier, S.J. Siegl, M. Vrabel, Mechanism-Based fluorogenic trans-Cyclooctene–Tetrazine cycloaddition, Angew. Chem., Int. Ed. 56 (2017) 1334–1337, https://doi.org/10.1002/ANIE.201610491.
[61] X. Shang, X. Song, C. Faller, R. Lai, H. Li, R. Cerny, W. Niu, J. Guo, Fluorogenic protein labeling using a genetically encoded unstrained alkene, Chem. Sci. 8 (2017) 1141–1145, https://doi.org/10.1039/C6SC03635J.
[62] J. Sauer, R. Sustmann, Mechanistic aspects of Diels-Alder Reactions: a Critical Survey, Angew Chem. Int. Ed. Engl. 19 (1980) 779–807, https://doi.org/10.1002/ANIE.198007791.
[63] C.A. Nixon, A.E. Thelen, M.A. Cordiner, Z. Kisiel, S.B. Charnley, E.M. Molter, J. Serigano, P.G.J. Irwin, N.A. Teanby, Y.-J. Kuan, Detection of cyclopropenylidene on Titan with ALMA, Astron. J. 160 (2020) 205, https://doi.org/10.3847/1538-3881/ABB679.
[64] J. Sauer, D.K. Heldmann, J. Hetzenegger, J. Krauthan, H. Sichert, J. Schuster 1, 2,4,5-Tetrazine: synthesis and Reactivity in [4+2] cycloadditions, Eur. J. Org Chem. 1998 (1998) 2885–2896, https://doi.org/10.1002/(SICI)1099-0690(199812)1998.
[65] D.R. Soenen, J.M. Zimpleman, D.L. Boger, Synthesis and inverse electron demand Diels-Alder reactions of 3,6-bis(3,4-dimethoxybenzoyl)-1,2,4,5-tetrazine, J. Org. Chem. 68 (2003) 3593–3598, https://doi.org/10.1021/JO020713V.
[66] L. Liu, M. Zang, L. Li, Y. Zhang, L. Wang, X. Zhou, C. Xin, X. Tai, MIL-53(Al)-derived bimetallic Pd–Co catalysts for the selective hydrogenation of 1,3-butadiene at low temperature, Sci. Rep. 15 (2025) 1–16, https://doi.org/10.1038/S41598-024-84707-3.
[67] T. Shittu, A.A. Dabbawala, L. Ali, A. Khaleel, M.Z. Iqbal, D.H. Anjum, K. Polychronopoulou, M. Altarawneh, Selective hydrogenation of 1,3-butadiene to butenes on ceria-supported Pd, Ni and PdNi catalysts: combined experimental and DFT outlook, Mater. Sci. Energy Technol. 8 (2025) 96–110, https://doi.org/10.1016/J.MSET.2024.11.001.
[68] L.M. Bickem, K. Gavriel, K. Neumann, Accessing functionalized tetrazines as click chemistry tools: a synthesis guide for chemists and chemical biologists, Eur. J. Org Chem. 27 (2024) e202301117, https://doi.org/10.1002/EJOC.202301117.
[69] Y. Feng, L. Zhou, Q. Wan, S. Lin, H. Guo, Selective hydrogenation of 1,3-butadiene catalyzed by a single Pd atom anchored on graphene: the importance of dynamics, Chem. Sci. 9 (2018) 5890–5896, https://doi.org/10.1039/C8SC00776D.
[70] M.J. Malaska, R. Hodyss, Dissolution of benzene, naphthalene, and biphenyl in a simulated Titan lake, Icarus 242 (2014) 74–81, https://doi.org/10.1016/J.ICARUS.2014.07.022.
[71] B.A. Younglove, J.F. Ely, Thermophysical properties of fluids. II. Methane, ethane, propane, isobutane, and normal butane, J. Phys. Chem. Ref. Data 16 (1987) 577–798, https://doi.org/10.1063/1.555785.
[72] K.A. Farley, K.H. Williford, K.M. Stack, R. Bhartia, A. Chen, M. de la Torre, K. Hand, Y. Goreva, C.D.K. Herd, R. Hueso, Y. Liu, J.N. Maki, G. Martinez, R. C. Moeller, A. Nelessen, C.E. Newman, D. Nunes, A. Ponce, N. Spanovich, P. A. Willis, L.W. Beegle, J.F. Bell, A.J. Brown, S.E. Hamran, J.A. Hurowitz, S. Maurice, D.A. Paige, J.A. Rodriguez-Manfredi, M. Schulte, R.C. Wiens, Mars 2020 Mission Overview, Space Sci. Rev. 216 (2020) 1–41, https://doi.org/10.1007/S11214-020-00762-Y.
[73] M.T. Taylor, M.L. Blackman, O. Dmitrenko, J.M. Fox, Design and synthesis of highly reactive dienophiles for the tetrazine-trans-cyclooctene ligation, J. Am. Chem. Soc. 133 (2011) 9646–9649, https://doi.org/10.1021/JA201844C.
[74] A. Grubisic, M.G. Trainer, X. Li, W.B. Brinckerhoff, F.H. van Amerom, R.M. Danell, J.T. Costa, M. Castillo, D. Kaplan, K. Zacny, Laser desorption mass spectrometry at Saturn's moon Titan, Int. J. Mass Spectrom. 470 (2021) 116707, https://doi.org/10.1016/J.IJMS.2021.116707.
[75] J.W. Wijnen, S. Zavarise, J.B.F.N. Engberts, M. Charton, Substituent effects on an inverse electron demand hetero Diels-Alder reaction in aqueous solution and organic solvents: cycloaddition of substituted styrenes to di(2-pyridyl)-1,2,4,5-tetrazine, J. Org. Chem. 61 (1996) 2001–2005, https://doi.org/10.1021/JO9518563.
[76] V. Poggiali, G. Brighi, A.G. Hayes, P.D. Nicholson, S. MacKenzie, D.E. Lalich, L. E. Bonnefoy, K. Oudrhiri, R.D. Lorenz, J.M. Soderblom, P. Tortora, M. Zannoni, Surface properties of the seas of Titan as revealed by Cassini mission bistatic radar experiments, Nat. Commun. 15 (2024) 1–10, https://doi.org/10.1038/s41467-024-49837-2.
[77] R.M.C. Lopes, M.J. Malaska, A.M. Schoenfeld, A. Solomonidou, S.P.D. Birch, M. Florence, A.G. Hayes, D.A. Williams, J. Radebaugh, T. Verlander, E.P. Turtle, A. Le Gall, S.D. Wall, A global geomorphologic map of Saturn's moon Titan, Nat. Astron. 4 (2020) 228–233, https://doi.org/10.1038/s41550-019-0917-6.
[78] S.M. Hörst, Titan's atmosphere and climate, J Geophys Res Planets 122 (2017) 432–482, https://doi.org/10.1002/2016JE005240.
[79] C.P. McKay, J.B. Pollack, R. Courtin, The greenhouse and antigreenhouse effects on Titan, Science 253 (1979) 1118–1121, https://doi.org/10.1126/science.11538492, 1991.
[80] L.R. Doose, E. Karkoschka, M.G. Tomasko, C.M. Anderson, Vertical structure and optical properties of Titan's aerosols from radiance measurements made inside and outside the atmosphere, Icarus 270 (2016) 355–375, https://doi.org/10.1016/j.icarus.2015.09.039.
[81] B. Reynard, F. Denat, B. Pedras, M.N.B. Santos, J.P. Farinha, C. Baleizão, System for inerting a fuel tank of an aircraft. Suitable for Calculating the Amount of Oxygen Contained in an Inerting Gas Injected into Said Tank, EP3176093B1, 2017.
[82] L. Bonaldi, M. Bortoluzzi, S. Zacchini, G. Pampaloni, F. Marchetti, L. Biancalana, Triazine chalcogenones from thiocyanate or selenocyanate addition to tetrazine ligands in ruthenium arene complexes, Inorg. Chem. 62 (2023) 7814–7833, https://doi.org/10.1021/ACS.INORGCHEM.3C00459.
[83] J. Brandrup, E.H. Immergut, W. McDowell, Polymer Handbook, Wiley, 1975.
[84] J.E. Mark, Polymer Data Handbook, Oxford University Press, 1999.